Open Ceramics 5 (2021) 100044

Contents lists available at ScienceDirect

Open Ceramics

journal homepage: www.editorialmanager.com/oceram

Sintering and phase formation of ceramics based on pre-treated municipal incinerator bottom ash

Alexander Karamanov [a,*], Emilia Karamanova [a], Luciana Maccarini Schabbach [b], Fernanda Andreola [c], Rosa Taurino [c], Luisa Barbieri [c]

[a] Institute of Physical Chemistry, Bulgarian Academy of Sciences, G. Bonchev Str. Block 11, 1113 Sofia, Bulgaria
[b] Univ Fed Santa Catarina, CERMAT Ceram & Composite Mat Res Grp, Campus Trindade, BR-88040900 Florianopolis, SC, Brazil
[c] Department of Engineering 'Enzo Ferrari', University of Modena and Reggio Emilia, Via P. Vivarelli 10, 41125 Modena, Italy

ARTICLE INFO

Keywords:
MIBA
Ceramics
Sintering
Thermal behavior
Optical dilatometry

ABSTRACT

Ceramics, based on 60 wt% of municipal incinerator bottom ashes (MIBA) and 40 wt% of industrial clays, were prepared by using two fractions of pre-treated ashes (above and under 2 mm) and three different industrial clays. The obtained six compositions with amounts of CaO from 12 to 14 wt%, with SiO_2/Al_2O_3 ratio ranging from 3.5 to 1.6 and with Al_2O_3/CaO ratio - from 1.25 to 1.75 were investigated and characterized.

These compositions were located in the crystallization field of anorthite ($CaO.Al_2O_3.2SiO_2$); the ceramics with high SiO_2/Al_2O_3 ratio are near to the eutectic with SiO_2, while with low ratio – closer to the anorthite stoichiometry.

The phase transformation and the subsequent melting were studied by non-isothermal DTA-TG analysis, while the densification process - by contactless optical dilatometry. Then, the optimal sintering temperatures and times were evaluated by isothermal dilatometric runs at different temperatures.

At high SiO_2/Al_2O_3 ratio the sintering temperature is lower but the sintering range is very narrow. This behavior can be explained by the formation of too high amount of liquid phase at the eutectic temperature. On the contrary, at lower ratio, the sintering temperature increases but, notwithstanding the decrease of viscosity and shorter sintering time, the densification range becomes wider. This last result is a very important technological finding with a view to industrial transferability.

Additional tests performed demonstrated that a preliminary thermal treatment of ash with elevated residual organic phase is necessary, which leads to a lower firing shrinkage and to a shorter sintering time.

1. Introduction

In recent years, the revaluation of "end-of-life" goods and products in the form of the return of materials to circulation is becoming increasingly widespread in the context of sustainable development policies. A sort of advanced recycling is such that the refusal of a process is not sent for disposal, but becomes raw material for another production cycle. This is the basic concept of the "technical nutrients" of the Circular Economy model, "an economy designed to regenerate itself, maintaining the value of products, materials and resources for as long as possible and returning them to the cycle of the product at the end of their use, minimizing waste generation" [1].

From the point of view of materials, the recycling of waste as well as the reuse of production and processing residues, allow its enhancement through technological innovation (both product and process). These actions are considered effective to reduce the dependence of the Europe by importing raw materials and improving the overall environment and the well-being of citizens.

Among the wastes that we can now consider wide-spread in most countries of the European community is the bottom ash of municipal solid waste incinerators, produced to the extent of about 30% of the waste placed in the combustion chamber. Moreover, the bottom ash represents a cost for the plants, being destined for disposal in landfills as non-hazardous waste with the 19 01 01 EWC (European Waste Code).

However, the bottom ash can be transformed into End of Waste after physical/mechanical treatments. This new product is an artificial siliceous aggregate, rich in Ca, Al and Fe, with different particle size distributions for different applications (cements, concretes, bricks, screeds

* Corresponding author.
E-mail address: karama@ipc.bas.bg (A. Karamanov).

https://doi.org/10.1016/j.oceram.2020.100044
Received 16 October 2020; Received in revised form 29 November 2020; Accepted 5 December 2020
Available online 17 December 2020

or ceramics). Thus these "new raw materials" can be used in the most advanced Green Building projects, thanks to their design compatibility, contributing to preserve natural raw materials and reducing CO_2 emission. Then, by the improvement of technological research, it is possible to create a final product with a high amounts of the recycled material. By using this new kind of raw material, it is also possible to obtain a final product with LEED (Leadership in Energy and Environmental Design) and BREEAM (British Research Environmental Assessment Method) certifications. In addition, the Action Plan for the Circular Economy of the European Commission (11 March 2020), has put in place a roadmap until 2022 with strategic and transversal actions to implement the Circular Economy, through:

1. A leading role in recycling, with expansion of the market for goods with recycled content;
2. Green Public Procurement "driving factor to increase the demand for sustainable products" (forecast of mandatory for products with recycled content);
3. Avoid "facade ecology" and admit only certifications, with requirements of independence and objectivity.

Among the procedures for the enhancement of the aforementioned bottom ashes are the preparation of glass-ceramics, ceramic, glasses, light weight aggregates and concrete [2–11]. The work proposed here is a part of a large study, addressed by the authors, in the same areas of materials [12–16].

Secondary Raw Material arising from municipal incinerator bottom ash (**MIBA**) was used. According to the European Waste Framework Directive (Directive 2008/98/EC) and subsequent amendments and additions, before the application of similar wastes as a source for different industrial manufactures, they can be pre-treated in order to transform the waste into a secondary raw material (known as End of Waste). In the case of **MIBA**, the treatment procedure is made of different crushing, grinding, screening, iron and metal removal processes, after which the product takes on the appearance of a sandy material. Depending on commercial applications, different grain sizes are produced, ranging from 0 to 12 mm, sometimes requiring wet refining processes. Usually, for the production of cement, brick and ceramic products, two grain sizes are required, below 2 mm (labeled **F** as fine) and above 2 mm (labeled **L** as large).

Firstly, we investigated glass-ceramics, obtained by low-cost "as it is" melting of the fine and the large ash fractions (i.e. without other additions in the batch), water quenching, milling of obtained frits and one step sinter-crystallization [12]. It was shown that, due to modest crystallization trend, **L** glass-ceramic sinter without significant difficulties in the temperature range 850–900 °C. At the same time, **F** glass-ceramic, which form higher amount of crystal phase, densify only in a narrow temperature range at about 1120 °C, which is near to the liquids temperature. In addition, the positive effect of inert atmosphere on the sinter-crystallization of the glass-ceramic by fine fraction was highlighted [13]. The improvements were explained by inhibited oxidation of FeO into Fe_2O_3, which leads to lower viscosity and inferior sintering temperature, coupled with variation in the phase composition and finer crystal size.

After that, well sintered ceramics were synthesized mixing 60 wt% of milled large or fine ash fractions with 40% kaolin, **K**. The optimal heat-treatments, the phase compositions, porosities and structures of the new ceramics (labeled **CLK** and **CFK**) were evaluated and discussed [14,15]. Semi-industrial samples were also obtained and characterized; the specimens show promising initial properties: bending strength of 40–45 MPa, Young's modulus of 40–45 GPa, high Mohs hardness and moderate thermal expansion coefficients.

Recently, toxicological and leaching tests for determination of the effectiveness of the sintering into glass-ceramics and ceramics were made [16]. Two microorganisms were used in the toxicological tests, *Escherichia coli* and *Staphylococcus aureus* (Agar Diffusion Test) and the results were compared with *Artemia sp*. (Acute Toxicity Test) and *Lactuca sativa* (germination).

Table 1
Chemical compositions of used clays and bottom ash fractions (wt. %).

	T	U	K	L	F
SiO_2	64.5	60.0	47.1	47.4	30.3
TiO_2	1.6	1.6	0.2	0.8	1.1
Al_2O_3	23.0	26.0	36.1	10.0	13.3
Fe_2O_3	1.1	1.0	1.0	4.4	10.8
CaO	0.2	0.4	0.4	18.8	20.8
MgO	0.3	0.6	0.3	2.9	2.8
K_2O	2.3	2.6	1.1	1.0	0.9
Na_2O	0.3	0.5	0.6	4.5	1.9
B_2O_3	0.0	0.0	0.0	0.6	0.3
MnO	0.0	0.0	0.0	0.3	0.8
ZnO	0.0	0.0	0.0	0.3	0.8
CuO	0.0	0.0	0.0	0.5	0.7
PbO	0.0	0.0	0.0	0.3	0.4
SO_3	0.0	0.0	0.0	1.0	1.7
P_2O_3	0.0	0.0	0.0	1.3	2.0
Chloride	0.0	0.0	0.0	0.0	0.5
Others	0.0	0.0	0.0	0.2	0.1
L.o.I	6.7	7.2	12.5	5.6	11.7

Regarding the leaching test, the sintering is confirmed to be a valid method to fix into the ceramic matrix alkali, anions and heavy metals, contained in this residue. Following the Italian regulation (in agreement with EU directives) about the waste landfilling, both ceramics can be classified as "not hazardous" but resulted non-inert materials for Cu and Pb. Regarding the toxicological tests, the bottom ash alone is mutagenic, but this effect disappeared once the ash is immobilized into glass-ceramics or ceramic tiles.

Here we summarize data for **CLK** and **CFK** ceramics with new results for other compositions, obtained by mixing of the fine and the large ash fractions with two different industrial clays. In these six ceramics the percentages of feldspars are minimal or these traditional fluxes practically absent. Practically, their compositions are somewhat similar to these of the glass-ceramics by industrial wastes [17,18], which however are characterized by significantly higher cost price. In addition, similar compositions formed high amount of crystal phase, which is a prerequisite for enhanced mechanical properties.

As a result, the densification mechanism is different from that in the traditional ceramics, where the formation of liquid phase is result mainly of the feldspar melting and the subsequent partial dissolution of quartz and metakaolin products [19–22]. These ceramics are also different from the several compositions, where waste glasses and industrial residues are used as alternative fluxes or inert addition [23–30].

The aim of our new report is to study the relationship between the phase formation and subsequent partial melting of formed crystal phases with the sintering. An explanation of the densification mechanism by the position of studied ceramics in the $CaO–Al_2O_3–SiO_2$ phase diagram is made. We hope that the results of this study are helpful to define the correct compositions and process parameters (holding temperature and time) for a possible industrial application of this new kind of materials.

2. Experimental

2.1. Materials

In this research, pre-treated municipal incinerator bottom ashes, coming from a plant of North of Italy, were recycled. In particular, two different fractions: **F**: fine (0–2 mm) and **L**: large (2–8 mm) were used. Two series of ceramics batches, containing 60 wt% of fine or large fractions, which were dry ground, milled and sieved below 75 μm, were prepared by mixing with 40 wt% of three different clays: kaolin ceramic grade (**K**), Ukraine clay (**U**) and German plastic clay (**T**). Thus six compositions were obtained, labeled as follow: **C** (by ceramics), **L** or **F** (depending on the used fraction) and **U**, **T** or **K** (depending on the used clay).

The results of chemical analysis, performed by Inductively Coupled Plasma, (ICP, Varian Liberty 200), of raw materials (expressed in oxides

Table 2
Chemical compositions of final ceramics (wt. %).

	CLT	CLU	CLK	CFT	CFU	CFK
SiO_2	57.8	56.0	51.7	48.8	47.0	42.2
TiO_2	1.2	1.2	0.6	1.4	1.4	0.8
Al_2O_3	16.2	17.5	22.3	19.1	20.5	25.6
Fe2O3	3.3	3.2	3.3	7.7	7.7	7.9
CaO	12.1	12.2	12.5	13.9	14.0	14.4
MgO	2.0	2.1	2.0	2.0	2.2	2.1
K_2O	1.6	1.7	1.1	1.6	1.8	1.1
Na_2O	3.0	3.1	3.2	1.4	1.5	1.6
B_2O_3	0.4	0.4	0.4	0.2	0.2	0.2
MnO	0.2	0.2	0.2	0.6	0.6	0.6
ZnO	0.2	0.2	0.2	0.6	0.6	0.6
CuO	0.3	0.3	0.3	0.5	0.5	0.5
PbO	0.2	0.2	0.2	0.2	0.2	0.2
SO_3	0.6	0.6	0.7	1.2	1.2	1.2
P_2O_3	0.8	0.8	0.8	1.3	1.3	1.3

wt%) are reported in Table 1, while in Table 2 are presented the resulting chemical composition of the investigated ceramics.

The silica amount is higher in **L** fraction, while CaO and Al_2O_3 - in **F** fraction. Also, the L.o.I. in the fine fraction is two times higher. In addition, as "fluxes" some alkaline and iron oxides are presented.

T and **U** clays contain higher amount of SiO_2 and lower content of Al_2O_3 respect to the kaolin **K**. The percentage of potassium is more than doubled while the quantities of other oxides are almost similar. Besides, the L.o.I is reduced from 12.5% in **K** to 6.7% and 7.2% in **T** and **U**, respectively.

The XRD analysis of raw materials (X'Pert PRO – Panalytical) demonstrated that both ash fractions mostly contain phases from melilite group (gehlenite-akermanite solid solutions), calcite, quartz, some plagioclase in form of albite solid solutions, as well as amorphous phase; the quartz amount is higher in the fine fraction, while calcite - in the fine fraction. The kaolin obviously contains mainly kaolinite with some traces of illite and quartz. In **U** and **T** clays the amount of kaolinite is lower and the quantity of illite and quartz (especially in **T**) is higher; traces of microcline are also identified.

2.2. Samples preparation

The mixtures were humidified (6 wt%) and pressing at 40 MPa using a uniaxial hydraulic press (Mignon C, Nannetti, Italy) to obtain bar samples (50x5x4 mm) suitable for firing in optical dilatometer.

The thermal behavior of batches was studied by non-isothermal DTA-TG analysis (Netzsch STA 409) at 20 °C/min and sample weight of about 100 mg.

The sintering trends were studied by non-isothermal treatment using a horizontal optical dilatometer (Expert System Solutions, Misura HSML ODLT 1400) at the same heating rate. In addition, in order to evaluate the optimal sintering temperatures and times, 1 h isothermal steps at selected temperatures were made.

The apparent, ρ_a, skeleton, ρ_s, and absolute, ρ_{as}, densities of the sintered samples at the optimal sintering temperature, as well as their water absorption, ***WA***, were determined and the results were used to evaluate closed, P_C, and open P_O porosity:

$$P_C = 100 \text{ x } \frac{\rho - \rho_s}{\rho_{as}} \quad (1)$$

$$P_O = WA \text{ x } \rho_a \quad (2)$$

ρ_a was estimated by precise micrometer, while ρ_s and ρ_{as} by gas pycnometer (AccyPy1330, Micromeritic) before and after crashing and milling the samples below 26 μm, respectively. ***WA*** was measured after 3 h boiling in distilled water and calculated by the following equation:

$$WA = \frac{ms - md}{md} * 100 \quad (3)$$

Where **ms** is saturated mass after boiling and **md** is dry mass.

3. Results and discussion

3.1. Non-isothermal heat-treatments

The studied ceramics contain SiO_2 from 42 to 56 wt%, Al_2O_3 from 16 to 26 wt%, as well as similar amounts of CaO (12–14 wt%). As a result, the ratio SiO_2/Al_2O_3 decrease significantly from 3.5 in **CLT** to 1.6 in **CFK**, while the ratio Al_2O_3/CaO varies from 1.25 to 1.75.

In Fig. 1-a the compositions of ceramics are plotted in the popular SiO_2–Al_2O_3–CaO phase diagram after recalculation to 100 wt% using these three main oxides. In addition, the compositions are simplified once more and are presented in the pseudo-binary diagram CaO.A-l_2O_3.2SiO_2–SiO_2 (see the inset). It can be assumed that the made approximations are acceptable because in the recalculations are used at about 80–85 wt% from all oxides, presented in the ceramics. Obviously, due to the laws of cryoscopy (i.e. the freezing point depression phenomenon), a substantial decreasing of both eutectic and liquids temperatures can be observed.

Fig. 1-a shows that all compositions are located in the crystallization field of anorthite (CaO.Al_2O_3.2SiO_2) and that the amount of this phase obviously can increase with the decrease of the ratio SiO_2/Al_2O_3. It is observed that the compositions **CLT** and **CLU** are close to the eutectic, while **CFK** is closer to the anorthite stoichiometry, which correspond to composition (wt %): SiO_2-43.2, Al_2O_3-36.6 and CaO-20.2; **CLK**, **CFT** and **CFU** are intermediate.

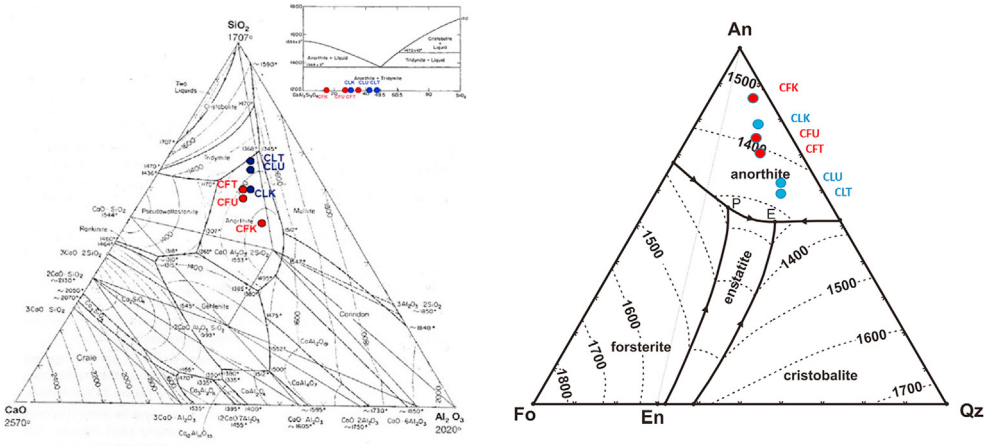

Fig. 1. a. The compositions studied on ternary phase diagram CaO–Al_2O_3–SiO_2. **b.** The compositions studied on ternary phase diagram silica, anorthite and forsterite.

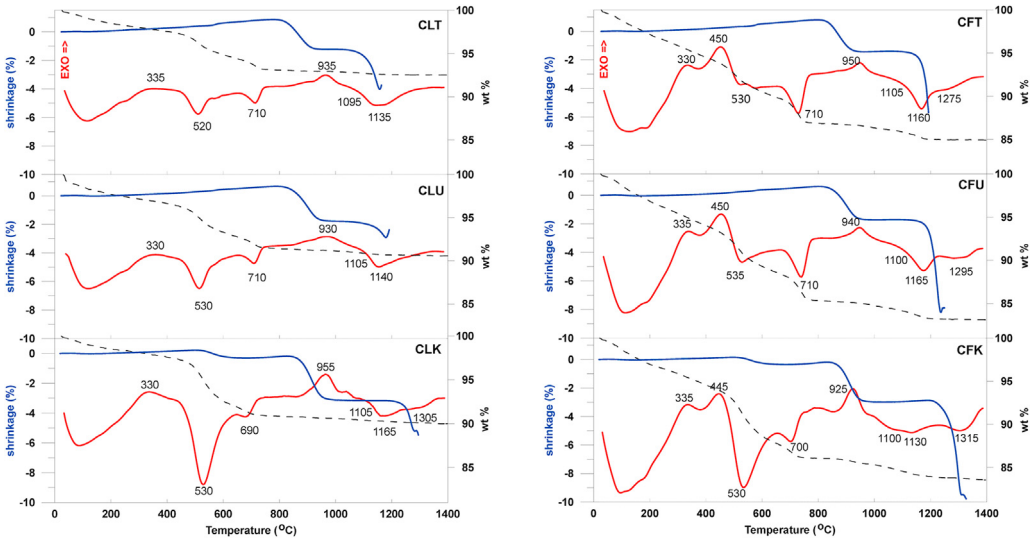

Fig. 2. Non-isothermal DTA, TG and sintering plots of **L** (a) and **F** (b) batches.

The studied compositions were also recalculated and presented in the phase diagram silica, anorthite and forsterite (see Fig. 1-b). In this case a half of the iron oxides and a half of the sodium oxide (in mol. %) were presented as MgO, assuming that they participate in the formation of pyroxene phase. The remaining iron and sodium oxides were presented as Al_2O_3, assuming the formation of anorthite solid solutions. In this manner in the recalculations were included more than 95% of all oxides in the ceramics.

The positions of studied ceramics in the crystallization field of anorthite in Fig. 1-b are similar to the results obtained with the simpler SiO_2–Al_2O_3–CaO phase diagram. It can be also noted that the last approximation correspond to the XRD results of final ceramics, which highlight a decreasing of crystallinity and anorthite amount with the decreasing of SiO_2/Al_2O_3 ratio, as well as presence of some quartz and pyroxene in the "eutectic" compositions. These XRD analysis, together with SEM observations of the structures of ceramics will be discussed in details in the second part of this study.

In Fig. 2-a and 2-b DTA-TG results for the batches, obtained using large or fine ash fractions are presented, respectively, together with the corresponding non-isothermals sintering plots. At low temperatures, due to the burning of organic rests, the DTA runs show exo-effects at about 330 and 450 °C, which are more intensive in the compositions based on fine fraction. The corresponding weight losses for **L** and **F** batches, are at about 3 and 7%, respectively, which is in agreement with the L.o.I. results, reported in Table 1. After that typical endo-effects at 530–550 °C, related to dihydroxylation of the clays and at 670–720°C, due to $CaCO_3$ decomposition, are presented. These reactions are confirmed by the TG losses and fit well with the phase compositions of used clay and waste materials. The greatest losses due to dihydroxylation are observed in both ceramics with kaolin, while the minimal losses are measured in the compositions with industrial clay **T**. In the same time, due to the higher amount of $CaCO_3$ in the fine fraction, the corresponding DTA and TG decomposition effects, are more intensive in the three **F** ceramics.

At higher temperatures in all batches are observed exo-effects with peaks at 930–950 °C, which are not linked with weight variations. These exothermal peaks can be associated with the formation of the anorthite phase, which is a result mainly of the reactions between metakaoline, arising from the clays, with CaO from the $CaCO_3$ and gehlenite from the bottom ash. In fact, the intensity of these effects are maximal in the compositions **CLK** and **CFK**, where pure kaolin is used. Similar effects are typical for the thermal behavior of various anorthite ceramics [31–33].

At temperatures above 1050 °C melting endo-effects are presented. In compositions **CLT** and **CLU** single endotherm, with peak temperatures at 1130–1140 °C, is evidenced. This effect is presented in all composition but its intensity diminishes with the decrease of the SiO_2/Al_2O_3 ratio. It is minimal in **CFK**, where in the range 1250–1400 °C more intensive second endotherm with peak temperature at ~1315 °C is observed. Similar second melting endo-effects, but with lower intensity and at inferior temperatures, are presented also in **CLK** and **CFU**. Indication for additional endo-effect might be observed in **CFT** too.

It can be assumed that the first endo-effect is due to formation of liquid phase at the eutectic temperature, while the second – because of melting of the remaining anorthite between the eutectic and liquidus temperatures. It can be also assumed that the eutectic temperature corresponds to the first onset of the primary endo-effect, whereas the liquidus temperature – to the peak temperature of the second endo-effect [34,35]. Despite the variations in chemical compositions, the six eutectic temperatures are very similar, at about 1100 °C, while the liquids temperatures increase with the decreasing of SiO_2/Al_2O_3 ratio. These results are in a good agreement with the preliminary analysis, showed in Fig. 1.

It can be also observed that the temperature ranges of the feldspar melting practically overlaps with the first endo effect. This means that the presence of some feldspars in the industrial clays **T** and **U** additionally will increase the rate of liquid phase formation and the related sintering process at the "eutectic" temperature.

The DTA-TG results are very helpful to study the sintering behavior. Up to 850 °C the dilatometric curves show only minor variations in **CLK** and **CFK** due to the kaolin dehydration and in **CLT** and **CFT** because of α-β quartz transformation. These results well fit with the phase analysis of used clays. Since the burning of residual organic matter and $CaCO_3$ decomposition are not related to volume changes, it can be assumed that these reactions lead to some increasing of the porosity.

In the interval, 850–950 °C all compositions shrink with 2–3% but this initial densification stops during the formation of anorthite phase. The final sintering obviously starts at higher temperatures after the formation of a sufficient amount of melt.

In the "eutectic" compositions **CLT** and **CLU** the sintering starts at lowest temperatures and completes near to the peak temperature of first endo-effect. After that, at low values of the reached shrinkage, deformation and expansion are observed, which is typical for samples forming a high amount of liquid phase. Contrary, in **CFK** no densification is observed after the formation of "eutectic" melt, because in this case the amount of this "primary" melt is significantly lower. In this composition the densification carries out in the interval 1250–1300 °C during the formation of addition liquids phase between the eutectic and the liquids temperatures. It can be assumed that, according to the lever rule, the

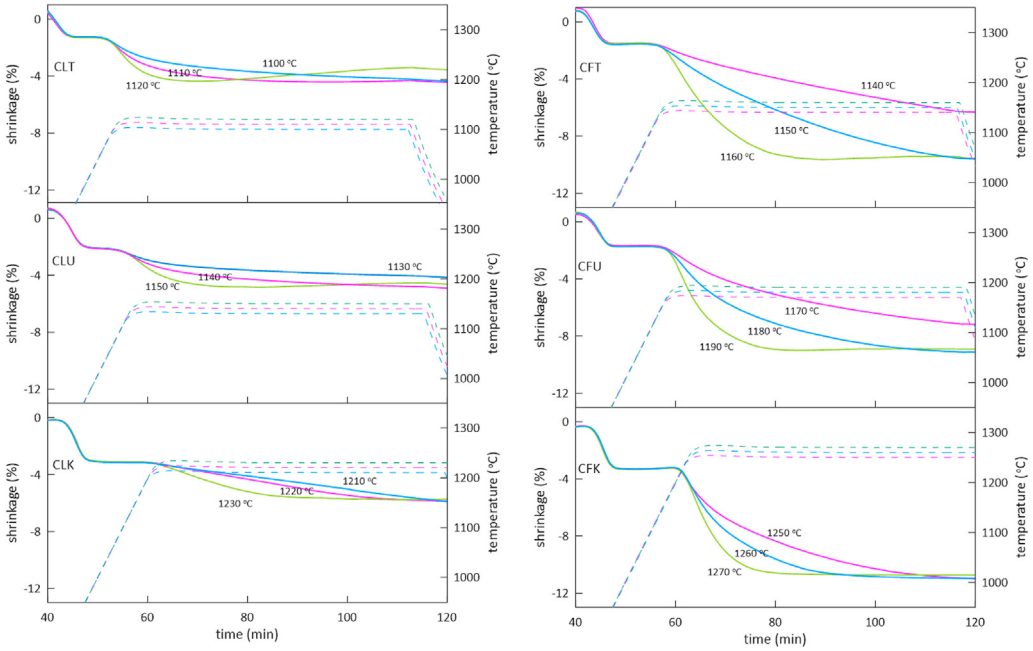

Fig. 3. Isothermal sintering plots of **L** (a) and **F** (b) ceramics.

amount of this "secondary" melt will increase gradually with the temperature due to the progressive melting of already formed anorthite. This means also that the amounts of Al_2O_3, CaO and SiO_2 in the liquid phase will increase with the temperate rise. Then, at higher temperatures, due to significant decreasing of the amount of crystal phase and diminishing of the viscosity is observed deformation.

The sintering behavior of the "intermediate" compositions **CLK**, **CFT** and **CFU** carries out at lower temperatures than in **CFK**. Notwithstanding in these ceramics the formed amount of "eutectic" melt also is not sufficient to complete the densification, so that the sintering carries out at temperatures higher than these of the first endotherm.

The made comparison of DTA and dilatometric results elucidate that the sintering temperature mainly depends on the position of ceramic composition in the used phase diagram. The closer the composition to the eutectic, the lower is its sintering temperature. In practice, the more "viscous" composition **CLT** (with higher sum SiO_2+Al_2O_3) sinter at a significantly lower temperature then less "viscous" composition **CFK** (with lower sum SiO_2+Al_2O_3). This intriguing difference can be explained with the rapid formation of high amount of liquid phase at the eutectic temperature in the first composition, and insufficient amount of "eutectic" melt – in the second one. This means that the sintering behavior depends mainly by the velocity of formation of liquid phase. Obviously, at lower viscosity of formed melt, the processes of the phase formation and dissolution will be accelerated. However, if its amount is not enough, the sintering process will be difficult. In addition, at lower viscosity the variation of phase composition with the temperature easier will "follow" the corresponding phase diagrams. Contrary, when the viscosity of formed liquid phase is too high, despite its amount, it is more difficult to rich the thermodynamic equilibria. An attempt to estimate and compare the viscosities and amounts of the melt phase, formed at the sintering temperatures, will be made in the second part of the work.

The described sintering behavior is different from that of the classic quartz-clay-feldspar ceramics. Notwithstanding that the main part of these traditional compositions is located in the primary field of mullite, it is difficult to explain their sintering behavior with the position in the phase diagram. In this case the sintering starts with the feldspars melting, but the increasing of the amount of liquid phase with the temperature usually is related to a partial dissolution of the quartz and the products of meta-kaolinite transformations. As a result, due to increasing of percentages of SiO_2 and Al_2O_3 in the liquid phase its viscosity also increases. This leads to a relatively large sintering intervals, which is a key technological advantage.

3.2. *Isothermal treatments*

The sintering temperature and time for each of the ceramics were evaluated after a series of isothermal experiments with the optical dilatometer. As optimal was assumed the temperature at which, after 1 h holding, the shrinkage rate becomes zero or close to zero and no significant overfiring (i.e. expansion of the samples) was observed. The results for ceramics, obtained with the large and fine ash fractions, are presented in Fig. 3-a and 3-b, respectively.

The optimal temperatures for the "eutectic" compositions **CLT** and **CLU** are 1110 and 1140 °C, respectively, and the reached shrinkages are only 4.5–5%. In **CLT** after ~ 40 min at 1110 °C starts some overfiring, while in **CLU** after 1 h at 1140 °C the densification process yet continues with a slow rate. However, at temperatures lower with 10 °C in both ceramics (especially in **CLU**) the sintering is uncompleted, whereas at higher with 10 °C – after 15–25 min starts overfiring, which is more intensive in **CLT**.

It can be concluded, that for these two compositions the sintering interval is very narrow and is close to the eutectic temperature. At lower temperatures the densification remains uncompleted due to the formation of insufficient percentage of liquid phase, while at higher temperatures, due to rapid formation of abundant amount of liquid phase, starts overfiring. Evidently, similar "eutectic" compositions are not very appropriated for an eventual industrial application.

The composition **CLK**, notwithstanding of higher with ~100 °C sintering temperature, demonstrates a more stable behavior within the temperature variations. In fact, after 1 h holding the three sintering plots practically overlap at shrinkage of about 6%. The sintering rates at 1210 and 1220 °C become zero after at about 30 and 60 min, respectively. At 1230 °C the densification process completes for only ~10 min, but the subsequent overfiring is negligible. It can be assumed that in this case drastic changes in the amount of formed liquid phase or/and in its viscosity are not observed within investigated temperature range.

The results with the isotherms of **F** ceramics confirm the higher shrinkages in comparison with **L** compositions. Notwithstanding, the

Table 3
Apparent (ρ_a), skeleton (ρ_s), and absolute (ρ_{as}) densities, water adsorption (**WA**) and the corresponding open (P_O), closed (P_C) and total (P_T) porosities of final ceramics.

Sample	Temperature (°C)	ρ_a (g/cm^3)	P_s (g/cm^3)	ρ_{as} (g/cm^3)	WA (%)	P_O (%)	P_C (%)	P_T (%)
CLT	1110	2.04	2.214	2.571	1.3	2.7	13.9	16.5
CLU	1140	2.02	2.287	2.668	2.3	4.6	14.3	18.9
CLK	1210	2.08	2.230	2.706	0.3	0.6	17.6	18.2
CFT	1150	2.12	2.518	2.790	3.1	6.6	9.7	16.3
CFU	1180	2.10	2.444	2.824	2.6	5.5	13.5	18.9
CFK	1260	2.16	2.348	2.822	0.4	0.9	16.8	17.7

sintering behavior of **CFT** is somewhat similar to that of the "eutectic" **CLT** and **CLU** ceramics, so that it also is unappropriated for the ceramic industry. In this case, the sintering range occurs at temperatures higher with only 30–40 °C than the corresponding eutectic temperature. At 1140 °C the sintering rate is low, at 1150 °C, which can be assumed as the optimal temperature for this composition, the sintering is not completed after 1 h, while at 1160 °C after 30–40 min starts slow overfiring.

In **CFU** the difference between the eutectic temperature and the sintering range increase and the variations between the three sintering plots are not so drastic as in **CFT**. At the optimal temperature of 1180 °C the sintering rate after 1 h holding is near zero, while at 1190 °C, where the densification completes for 20–30 min, the overfiring trend is negligible.

Finally, in **CFK**, even if the shrinkage is highest (about 11%), the three sintering curves overlaps and a tendency for overfiring is not observed. The optimal sintering temperature of this ceramic is at about 1260 °C and the sintering time is 30–40 min.

The reported results confirm that the sintering behavior strongly depends on the position of ceramic composition in the phase diagram. If it is near to a eutectic a big amount of liquid phase will be formed in a narrow temperature interval; as a result, similar compositions are not technological.

Contrary, if the composition is closer to the stoichiometry of the main crystalline phase, the amount of formed melt will increase gradually with the temperature rise. In the case of anorthite as main crystal phase, the amount of SiO_2, Al_2O_3 and CaO in the melt will increase. This have a positive effect against the tendency for deformation, because a significant drop of the melt viscosity is not expected with some temperature rise. Obviously, this effect of "auto-regulations" is not so strong as this in the traditional ceramics, where the primary feldspar melt dissolve quartz and meta-kaolin and thus the viscosity increasing is significant.

Somewhat similar data were reported in another our work [36], where three ceramic batches, containing no feldspar, 30 wt % kaolin, 30, 50 and 70 wt% blast furnace slag and 40, 20 and 0 wt% quartz sand, respectively, were studied. The composition with 30% slag was located in the field of silica phases, so that the quartz dissolution was inhibited and the sintering rate was relatively low. The composition with 50% slag was "eutectic" and was characterized with very narrow sintering interval, high sintering rate and, as a result, with a tendency for fast deformation. At the same time, the composition with 70% slag was non-eutectic and, notwithstanding of the lowest amount of SiO_2 and the lower viscosity, was more technological, formed higher amount of crystal phases and shown the best mechanical properties.

3.3. Burn out effect

It was already noted that the final shrinkages in the ceramics with fine ash fraction are significantly higher (with 4–5%) than in the corresponding ceramics with large fraction. If all "green" samples are characterized with similar porosities before the beginning of densification, this difference can indicate that the **F** ceramics are sintered significantly better.

In order to highlight this particularity, the porosities (both open and closed) of the samples, heat-treated at the optimal temperatures, were measured by water soaking tests and pycnometric measurements, respectively.

The results for water adsorption, apparent, skeleton and absolute densities, as well as these for the resulting open and closed porosities are summarized in Table 3. This data demonstrates an acceptable degree of sintering for all samples and total porosities between 16 and 19%. According to values for water adsorption [37] **CFK** and **CLK** belong to BIa Group (≤0.5%) while **CLT**, **CLU**, **CKT** and **CKU** ceramics belong to BIb Group (0.5–3%). These low values permit to identify eventual application of similar ceramic as wall and floor tiles.

The occurrence of 5–6% open porosity in **CLU**, **CFU** and **CFT** indicates that the sintering in these composition is not entirely completed and that probably longer holding time is necessary. This fits well with the isothermal sintering curves and perhaps is related to a relatively high viscosity of the formed liquid phases at the applied low sintering temperature.

In other three compositions the water soaking values are lower and the sintering rate becomes zero after 30–40 min; however, the measured percentages of closed porosities are relatively high. In fact, in the well sintering ceramics with zero water adsorption (as porcelain stoneware) the closed porosity is at about two-three times lower [20,38].

Probably, the high closed porosity in **CLT** can be partially related to the trend for overfiring in this "eutectic" compositions. However, in **CLK** and **CFK** a tendency for overfiring is not observed, so that the higher closed porosity might be explained mainly with re-crystallization of a part of anorthite (i.e. due to low viscosity and high precipitation a part of melted at heating anortihite is formed again at cooling). Because of increasing of the density during crystallization, this phase formation leads to the creation of some additional crystallization induced porosity [13,14,39,40]. This phenomenon will be discussed in details in the second part of this study.

It can be concluded that the total porosity in all specimens does not change so significantly to explain the observed big difference in the firing shrinkages. So that, it can be assumed that extra porosity is formed in the "greens" mainly during the burning of organic residues from the ashes before the beginning of the sintering. Obviously, this additional porosity can be higher in ceramics base on fine ash fraction, where the L.o.I and the firing shrinkage are higher.

In order to confirm this statement some additional tests were made with the most promising **CFK** and **CLK** ceramics.

Firstly, the apparent densities of dried initial samples were measured before and after heat-treatment to 800 °C. This temperature guarantees the burning of organic fraction, dihydroxylation of the clays and decomposition of $CaCO_3$, but is too low for densification and anorthite formation. The results show that after this heat-treatment the density in **CLK** decreases from ~1.86 g/cm^3 to ~1.69 g/cm^3, which corresponds to the formation of at about 9% new porosity. In **CFK**, the density decreases from ~1.83 g/cm^3 to ~1.55 g/cm^3, which means that the formed additional porosity is at about 16%. At the same time, reasonably the firing shrinkages were very low: ~ 0.4% in **CFK** and ~ 0.5 in **CLK**.

Then, in order to improve the sintering and to decrease the firing shrinkage other experiments were made using new portions of the large and the fine ash fractions. These samples were pre-treated for 1 h at 600 °C to guarantees the fully burning of the organic rests. As a result, L.o.I. in the large fraction decrease from ~7 to ~3% and in the fine fraction – from ~12 to ~3%.

After that 60 wt% of thus obtained pre-heat treated ashes (labeled as **L-b** and **F-b**, respectively) were mixed with 40 wt% of **K** to obtain two

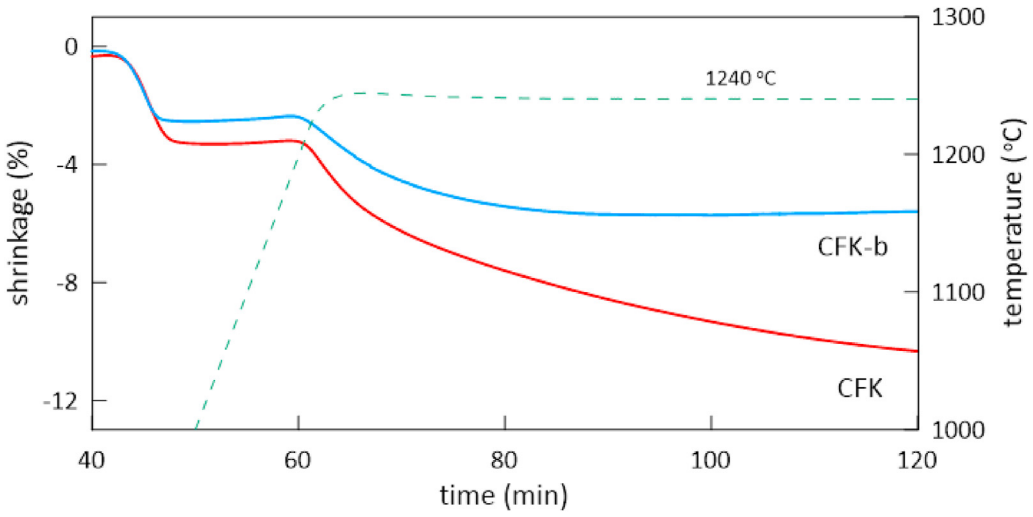

Fig. 4. Isothermal sintering plots of **CFK** and **CFK-b** at 1240 °C.

new batches: **CLK-b** and **CFK-b**. The new "green" samples were prepared identically to all other ceramics.

The DTA results of **CLK-b** and **CFK-b** mixes logically doesn't show exo-effects and weight losses in the interval 300–500 °C, while all other effects were similar to these in **CLK** and **CFK**. At the same time, the sintering dilatometric curves demonstrate evident differences.

In **CFK-b** a significant decreasing of the firing shrinkage is observed, combined with some reduction of the sintering temperature with ~ 20 °C. This is elucidated in Fig. 4, where are compared the sintering results at 1240 °C for **CFK** and **CFK-b**. It is well seen that the preliminary burn-out of **F** fraction leads to very positive technological results. The total firing shrinkage decreases with at about 6%, which means that the trend for eventual deformation during the sintering is eliminated. In addition, the lower shrinkage reduces the sintering time, which means that the energy consumption for the preliminary burn-out (if there are no other possibilities to eliminate the organic rests) might be partially compensated by the shorter firing times.

The preliminary burn-out of the large fraction also decreases the firing shrinkage in **CLK-b**, but in this case the effect is below 2%. However, contrarily to **CFK-b**, in **CLK-b** the improvement of the densification is observed mainly in the low temperature interval between 900 and 1050 °C; in the range 1200–1250 °C the firing shrinkage is only at about 1%. This behavior is demonstrated in Fig. 5, where together are presented the non-isothermal sintering plots of **CLK-b** and **CLK**.

The interesting improvement of the densification in the low temperature range contributed our additional studies with compositions, based on **CLK-b**. As a result, samples were obtained after only 5–10 min holding at 1000 °C [41]. The characteristics of these ceramics overcome ones of the traditional masonry bricks, which was explained with the anorthite formation due to the intensive reactions between meta-kaolinite and pre heat-treated large fraction. In a subsequent research the positive effect of microwave heat-treatment on the structure and properties were also studied [42]. It was demonstrated that the used microwave hybrid heating leads to a decreasing of firing temperature with about 100 °C and to an additional improvement of the mechanical performance.

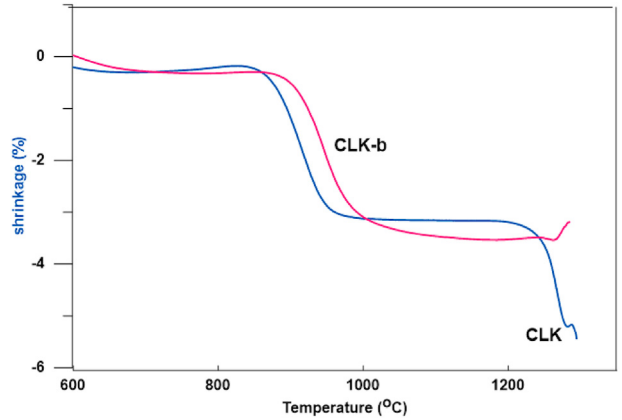

Fig. 5. Non-isothermal sintering plots of **CLK** and **CLK-b**.

4. Conclusions

Ceramics, based on 60 wt% municipal incinerator bottom ashes and 40 wt% of industrial clays are studied. The compositions investigated contain SiO_2 between 42 and 58 wt%, Al_2O_3 between 16 and 26 wt% and CaO between 12 and 14 wt%. As a result, the sintering mechanism is different with respect to a traditional ceramic, where the liquid phase is formed by the feldspar melting and partial dissolution of quartz and clay phases transformations.

It is demonstrated that the densification behavior of studied ceramics can be reasonable explained by their position in the $CaO–Al_2O_3–SiO_2$ phase diagram. When the composition is near to the eutectic it is not appropriated for industrial application due to narrow sintering range. Contrary, when the composition is closer to the anorthite stoichiometry it is more technological, despite the sintering temperature is higher and the sintering time is shorter.

It is also highlighted that, when the content of organic residues in the ash is high, its preliminary thermal pre-treatment is necessary to decrease the firing shrinkage and then to obtain a shorter sintering time.

Declaration of competing interest

The authors declare that they have no known competing financial interests or personal relationships that could have appeared to influence the work reported in this paper.

Acknowledgments

A. Karamanov and E. Karamanova express their gratitude for the financial support of Project BG05M2OP001-1.002-0019: "Clean technologies for sustainable environment—waters, waste, energy for circular economy." All authors are also thankful for the support for realization of the experimental setup of the Bulgarian Science Fund (FNI) under Project DN 19/7 "Theory and application of sinter-crystallization."

References

[1] Ellen MacArthurFoundation. https://www.ellenmacarthurfoundation.org/explore/the-circular-economy-in-detail.consulted Sept.2020.

[2] E. Rambaldi, L. Esposito, F. Andreola, L. Barbieri, I. Lancellotti, I. Vassura, The recycling of MSWI bottom ash in silicate based ceramic, Ceram. Int. 36 (2010) 2469–2476, https://doi.org/10.1016/j.ceramint.2010.08.005.

[3] L. Barbieri, A. Corradi, I. Lancellotti, T. Manfredini, Use of municipal incinerator bottom ash as sintering promoter in industrial ceramics, Waste Manag. 22 (2002) 859–863, https://doi.org/10.1016/j.ceramint.2010.08.005.

[4] C.H.K. Lam, A.W.M. Ip, J.P. Barford, G. McKay, Use of incineration msw ash: a review, Sustainability 2 (2010) 1943–1968, https://doi.org/10.3390/su2071943.

[5] C.R. Cheeseman, S. Monteiro da Rocha, C. Sollars, S. Bethanis, A.R. Boccaccini, Ceramic processing of incinerator bottom ash, Waste Manag. 23 (2003) 907–916, https://doi.org/10.1016/S0956-053X(03)00039-4.

[6] R.V. Silva, J. de Brito, C.J. Lynn, R.K. Dhir, Environmental impacts of the use of bottom ashes from municipal solid waste incineration: a review, Resour. Conserv. Recycl. 140 (2019) 23–35, https://doi.org/10.1016/j.resconrec.2018.09.011.

[7] A. Bourtsalas, L.J. Vandeperre, S.M. Grimes, N. Themelis, C.R. Cheeseman, Production of pyroxene ceramics from the fine fraction of incinerator bottom ash, Waste Manag. 45 (2015) 217–225, https://doi.org/10.1016/j.wasman.2015.02.016.

[8] N.L. Ferber, D.P. Minh, Q. Falcoz, A. Meffre, N. Tessier-Doyen, A. Nzihou, V. Goetz, Ceramics from municipal waste incinerator bottom ash and wasted clay for sensible heat storage at high temperature, Waste and Biomass Valorization (2019) 1–14. https://hal-mines-albi.archives-ouvertes.fr/hal-02049781.

[9] M. Romero, R.D. Rawlings, J.Ma Rincón, Development of a new glass–ceramic by means of controlled vitrification and crystallisation of inorganic wastes from urban incineration, J. Eur. Ceram. Soc. 19 (1999) 2049–2058, https://doi.org/10.1016/S0955-2219(99)00011-4.

[10] S. Bethanis, C.R. Cheeseman, in: V. Popov, H. Itoh, C.A. Brebbia, S. Kungolos (Eds.), Production of Lightweight Aggregate from Incinerator Bottom Ash and Pulverised Fuel Ash, Waste Management and the Environment II, WIT Press, 2004. www.witpress.com, 1-85312-738-8.

[11] M. Ferraris, M. Salvo, A. Ventrella, L. Buzzi, M. Veglia, Use of vitrified MSWI bottom ash for concrete production, Waste Manag. 29 (2009) 1041–1047, https://doi.org/10.1016/j.wasman.2008.07.014.

[12] L. Schabbach, F. Andreola, E. Karamanova, I. Lancellotti, A. Karamanov, L. Barbieri, Integrated approach to establish the sinter-crystallisation ability of glasses from secondary raw material, J. Non-Cryst. Solids 357 (2011) 10–17, https://doi.org/10.1016/j.jnoncrysol.2010.10.006.

[13] A. Karamanov, L.M. Schabbach, E. Karamanova, F. Andreola, L. Barbieri, B. Ranguelov, G. Avdeev, I. Lancellotti, Sinter-crystallization in air and inert atmospheres of a glass from pre-treated municipal solid waste bottom ashes, J. Non-Cryst. Solids 389 (2014) 50–59, https://doi.org/10.1016/j.jnoncrysol.2014.02.009.

[14] L.M. Schabbach, F. Andreola, L. Barbieri, I. Lancellotti, E. Karamanova, B. Ranguelov, A. Karamanov, Post-treated incinerator bottom ash as alternative raw material for ceramic manufacturing, J. Eur. Ceram. Soc. 32 (2012) 2843–2852, https://doi.org/10.1016/j.jeurceramsoc.2012.01.020.

[15] F. Andreola, L. Barbieri, I. Lancellotti, L.M. Schabbach, E. Karamanova, A. Karamanov, Building ceramic products obtained from refractory clay and post-treated MSW bottom ash, Tiles & Bricks International 2 (2012) 33–41.

[16] F. Andreola, L. Barbieri, B. Queiroz Soares, A. Karamanov, L.M. Schabbach, A.M. Bernardin, C.T. Pich, Toxicological analysis of ceramic building materials – tiles and glasses – obtained from post-treated bottom ashes, Waste Manag. 98 (2019) 50–57, https://doi.org/10.1016/j.wasman.2019.08.008.

[17] I.W. Donald, Waste Immobilization in Glass and Ceramics Based Hosts, Vitrification of Nonradioactive Toxic and Hazardous Wastes, Wiley, 2010.

[18] R.D. Rawlings, J.P. Wu, A.R. Boccaccini, Glass-ceramics: their production from wastes - a review, J. Math. Sci. 41 (2006) 733–761. https://doi:10.1007/S10853-006-6554-3.

[19] C. Zanelli, M. Raimondo, G. Guarini, M. Dondi, The vitreous phase of porcelain stoneware: composition, evolution during sintering and physical properties, J. Non-Cryst. Solids 357 (16–17) (2011) 3251–3260, https://doi.org/10.1016/j.jnoncrysol.2011.05.020.

[20] C. Zanelli, M. Raimondo, M. Dondi, G. Guarini, P. Tenorio, Sintering mechanisms of porcelain stoneware tiles, M. o. Qualicer (2004) 247–259.

[21] J. Martín-Márquez, J.M. Rincón, M. Romero, Effect of firing temperature on sintering of porcelain stoneware tiles, Ceram. Int. 34 (2008) 1867–1873, https://doi.org/10.1016/j.ceramint.2007.06.006.

[22] T. Manfredini, G.C. Pellacani, M. Romagnoli, Porcelain stoneware tiles, Am. Ceram. Soc. Bull. 74 (5) (1995) 76–79. ISSN 0002-7812.

[23] M. Raimondo, C. Zanelli, F. Matteucci, G. Guarini, M. Dondi, J.A. Labrincha, Effect of waste glass (TV/PC cathodic tube and screen) on technological properties and sintering behaviour of porcelain stoneware tiles, Ceram. Int. 33 (2007) 615–623, https://doi.org/10.1016/j.ceramint.2005.11.012.

[24] F. Matteucci, M. Dondi, G. Guarini, Effect of soda-lime glass on sintering and technological properties of porcelain stoneware tiles, Ceram. Int. 28 (2002) 873–880, https://doi.org/10.1016/S0272-8842(02)00067-6.

[25] G. Carbonchi, M. Dondi, N. Morandi, F. Tateo, Possible use of altered volcanic ash in ceramic tile production, Ind. Ceram. 19 (1999) 67–74.

[26] S. Ergul, M. Akyildiz, A. Karamanov, Ceramic material from basaltic tuffs, Ind. Ceram. 37 (2007) 75–80.

[27] F. Andreola, L. Barbieri, E. Karamanova, I. Lancellotti, M. Pelino, Recycling of CRT panel glass as fluxing agent in the porcelain stoneware tile production, Ceram. Int. 34 (2008) 1289–1295, https://doi.org/10.1016/j.ceramint.2007.03.013.

[28] P. Torres, H.R. Fernandes, S. Agathopoulos, D.U. Tulyaganov, J.M.F. Ferreira, Incorporation of granite cutting sludge in industrial porcelain tile formulations, J. Eur. Ceram. Soc. 24 (2004) 3177–3185, https://doi.org/10.1016/j.jeurceramsoc.2003.10.039.

[29] L.A. Diaz, R. Torrecillas, Porcelain stoneware obtained from the residual mud of serpentinite raw materials, J. Eur. Ceram. Soc. 27 (2007) 2341–2345, https://doi.org/10.1016/j.jeurceramsoc.2006.07.023.

[30] P. Torres, R.S. Manjate, S. Quaresma, H.R. Fernandes, J.M.F. Ferreira, Development of ceramic floor tile compositions based on quartzite and granite sludges, J. Eur. Ceram. Soc. 27 (2007) 4649–4655, https://doi.org/10.1016/j.jeurceramsoc.2006.07.023.

[31] K. Traoré, T. Kabré, P. Blanchart, Gehlenite and anorthite crystallization from kaolinite and calcite mix, Ceram. Int. 29 (2003) 377–383, https://doi.org/10.1016/S0272-8842(02)00148-7.

[32] A. Mergen, T.S. Kayed, M. Bilen, A.F. Qasrawi, M. Gürü, Production of anorthite from kaolinite and CaCO3 via colemanite, Key Eng. Mater. 264 (2004) 1475–1478. https://10.4028/www.scientific.net/kem.264-268.1475.

[33] P. Ptáček, T. Opravil, F. Šoukal, J. Havlica, R. Holešinský, Kinetics and mechanism of formation of gehlenite, Al–Si spinel and anorthite from the mixture of kaolinite and calcite, Solid State Sci. 26 (2013) 53–58, https://doi.org/10.1016/j.solidstatesciences.2013.09.014.

[34] J. Šesták, Heat, Thermal Analysis and Society, 2004. Nucleus HK, Praha, Czech Republic.

[35] Ji-Cheng Zhao, Methods for Phase Diagram Determination, Elsevier Science, Amsterdam, 2007.

[36] E. Karamanova, G. Avdeev, A. Karamanov, Ceramics from blast furnace slag, kaolin and quartz, J. Eur. Ceram. Soc. 31 (2011) 989–998, https://doi.org/10.1016/j.jeurceramsoc.2011.01.006.

[37] ISO 13006 - Ceramic Tiles – Definitions, Classification, Characteristics and Marking, International Organization for Standardization, 2018.

[38] M. Romero, J.M. Perez, Relation between the microstructure and technological properties of porcelain stoneware, A review, Materiales de Construcción. 65 (2015), https://doi.org/10.3989/mc.2015.05915.

[39] A. Karamanov, M. Pelino, Induced crystallization porosity and properties of sintered diopside and wollastonite glass-ceramics, J. Eur. Ceram. Soc. 28 (2008) 555–562, https://doi.org/10.1016/j.jeurceramsoc.2007.08.001.

[40] V.M. Fokin, A. Karamanov, A.S. Abyzov, J.W.P. Schmelzer, E.D. Zanotto, Stress-induced pore formation and phase selection in a crystallizing stretched glass, in: Jurn W.P. Schmelzer (Ed.), Glass - Selected Properties and Crystallization, De Gruyter, 2014, pp. 441–479.

[41] R. Taurino, E. Karamanova, L. Barbieri, S. Atanasova-Vladimirova, F. Andreola, A. Karamanov, New fired bricks based on municipal solid waste incinerator bottom ash, Waste Manag. Res. 35 (2017) 1055–1063. https://doi: 10.1177/0734242X17721343.

[42] R. Taurino, A. Karamanov, R. Rosa, E. Karamanova, L. Barbieri, S. Atanasova-Vladimirova, G. Avdeev, C. Leonelli, New ceramic materials from MSWI bottom ash obtained by an innovative microwave-assisted sintering process, J. Eur. Ceram. Soc. 37 (2017) 323–331, https://doi.org/10.1016/j.jeurceramsoc.2016.08.011.